RSC Advances

Journal Name RSCPublishing

ARTICLE

The effect of growth oxygen pressure on the metal-insulator transition of ultrathin $Sm_{0.6}Nd_{0.4}NiO_{3-\delta}$ epitaxial films

Cite this: DOI: 10.1039/x0xx00000x

Received 00th January 2012, Accepted 00th January 2012

DOI: 10.1039/x0xx00000x

www.rsc.org/

Haoliang Huang [a, b, c], Zhenlin Luo [b, c, *], Yuanjun Yang [b, c], Mengmeng Yang [b, c], Haibo Wang [b, c], Guoqiang Pan [b], Yalin Lu [c], and Chen Gao [a, b, c, *]

Ultrathin $Sm_{0.6}Nd_{0.4}NiO_{3-\delta}$ epitaxial films were deposited by pulsed laser deposition (PLD) onto $LaAlO_3$ (LAO) single crystal substrates. The influence of growth oxygen pressure on the metal-insulator transition (MIT) was investigated. It was found that the MI transition temperature (T_{MI}) of the films decreases remarkably with the decrease of the growth oxygen pressure, while the films' strain state keeps almost the same. The increased oxygen vacancies induced by lower growth oxygen pressure, verified by x-ray photoelectron spectroscopy, seem to be the main cause of such phenomena.

Introduction

As a classical correlated system with metal-insulator transition (MIT), the perovskite nickelates (*Re*NiO_3, *Re* is trivalent rare earth ion but not La) have attracted great interest due to the coupling of charge and magnetic orders in the insulating region, which suggests some of them might be magnetoelectric multiferroics [1-4]. Bulk *Re*NiO_3 is insulating monoclinic at low temperature, and transfers to metallic orthorhombic phase as temperature increases above the critical metal-insulator transition temperature (T_{MI}). The change in resistivity around T_{MI} can be 2-3 orders of magnitude across a narrow temperature window (~10 K) [5]. And there are wide ranging of possible applications, from sensors, optoelectronic switches to memory [6]. The MIT of these *Re*NiO_3 can be tuned continuously by excitation such as pressure [7], electrical field [8, 9, 10], epitaxial strain [7, 11, 12], and nonstoichiometry [13]. It is believed that these excitations distort the Ni-O-Ni angle from 180°, and therefore shift the MIT to a higher temperature [1]. The *Re*NiO_3 are hard to be synthesized in bulk because where the nickel must adopt the less stable Ni^{3+} oxidation state, which requires high oxygen pressure processing. However, it is relatively easy to fabricate *Re*NiO_3 as epitaxial thin films at low pressure. The presence of unstable Ni^{3+} oxidation state implies the possibility of large oxygen nonstoichiometry in *Re*NiO_3 thin films. Actually, the oxygen vacancies can greatly affect the structural, magnetic and transport properties of the *Re*NiO_3[5, 14, 15]. Although it seems that vacancies always increase the resistivity of the metallic state and make the MIT less sharp [16], it is still unclear whether the oxygen vacancies increase the T_{MI} or leave it unaffected [17], because it is difficult to rule out the effect of strain from that of oxygen vacancy. For example, in $NdNiO_3$ epitaxial films grown on $SrTiO_3$, tensile strain in the film causes more oxygen vacancies and more flat MIT [18].

From an electronic application viewpoint, the materials with sharp transition around room temperature are noteworthy [19]. It is reported that $Sm_{1-x}Nd_xNiO_3$ films grown on $NdGaO_3$ substrate show a systematic change in T_{MI}, from 199 K for x=1 to 378 K for x=0 [13], and the transition of $Sm_{0.6}Nd_{0.4}NiO_3$ takes place near room temperature. In this letter, we report on the influence of growth oxygen pressure on the transport property of $Sm_{0.6}Nd_{0.4}NiO_{3-\delta}$ (SNNO) ultrathin films. As far as possible to avoid the strain effect, we studied almost fully-strained SNNO films grown on $LaAlO_3$ (LAO) substrates, where the lattice mismatch is only -0.4%. It is found that the T_{MI} is remarkably decreased from 365 to 220 K, when the growth oxygen pressure varied from 25 to 10 Pa. Meanwhile the valence state of Ni is changed, whereas the crystal lattice of SNNO changes slightly. It is inferred that different growth oxygen pressure results in varied oxygen vacancy content in the film, and the transport properties are the joint effect of the changes of Ni valence, elongation of Ni-O bond length, bending of Ni-O-Ni angle and the formation of $Ni^{3-\delta}$-O^{2-}-$Ni^{3+\delta}$ charge ordering.

Experimental

Thin film preparation

Epitaxial SNNO thin films were deposited by pulsed laser deposition (PLD) using a KrF excimer laser (λ=248 nm, Coherent Inc.) at pulse frequency of 5 Hz and power density of 1 J/cm^2. In order to minimize the strain effect, (001)-oriented LAO single crystal substrates (a=0.379 nm, PDF No. 85-0848) were used. A sintered stoichiometric SNNO tablet was used as the target. Before film growth, the chamber was pumped to a pressure on the order of 10^{-4} Pa, then backfilled with pure oxygen to 10, 20 and 25 Pa, respectively. During the deposition, the substrate was maintained at a temperature of 600°C (using resistance heating silk). After film growth, the samples were annealed *in situ* for 30 min before cooling down to room temperature at a rate of 5°C/min. The parameters were kept the same for different depositions to ensure the change in transition temperature is mainly caused by the change of growth oxygen pressure.

Characterization

The temperature-dependent resistance measurement of the films was carried out from 100 K to 400 K on a He-compression cryogenic device (ARS-2HW) with standard four-probe method. In order to obtain Ohmic contact, Au contacts were sputtered onto the top of the sample through a shadow mask. Thickness of films was estimated by X-ray reflectivity (XRR) at the beam line BL14B1 of Shanghai Synchrotron Radiation Facility (SSRF, λ=1.2398 Å). The crystalline quality and lattice parameters were measured by high resolution synchrotron X-ray diffraction at U7B beam line of the National Synchrotron Radiation Laboratory (NSRL, λ=1.537 Å). To measure the in-plane lattice parameters, grazing incidence X-ray diffraction (GIXRD) was performed on a four-circle diffractometer with a Ge (220) × 2 incident-beam monochromator (Rigaku SmartLab Film Version with an in-plane arm for GIXRD, Cu-*Kα* radiation). X-ray photoelectron spectroscopy (XPS) analyses were performed using an ESCALAB 250 system (Thermo Scientific).

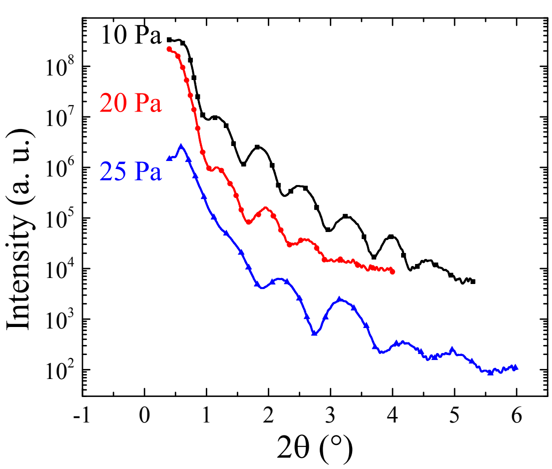

Figure 1 XRR analysis of films deposited under 10 Pa, 20 Pa, and 25 Pa, respectively.

Results and discussion

The small angle x-ray reflection patterns of the samples deposited under 10 Pa, 20 Pa, and 25 Pa are shown in Fig. 1. All the x-ray reflection patterns show distinctive Kiessig fringes, and the corresponding thickness could be calculated according to the following Bragg equation modified for refraction index [20, 21]

$$n\lambda = 2d\left(\theta_n^2 - \theta_c^2\right)^{1/2}, \quad (1)$$

where, d is the film thickness, θ_n is the angle of the nth fringe, and θ_c is the critical angle for the film. The respective thickness of the films deposited under 10, 20 and 25 Pa are estimated to be 10, 10.5 and 7.8 nm, respectively, which are far less than the critical value for strain relaxation (about 47.5 nm, 125 u. c.). From the fringes, we can also qualitatively learn that the roughness of the film deposited under 10 Pa is smaller than that of the films deposited under 20 and 25 Pa.

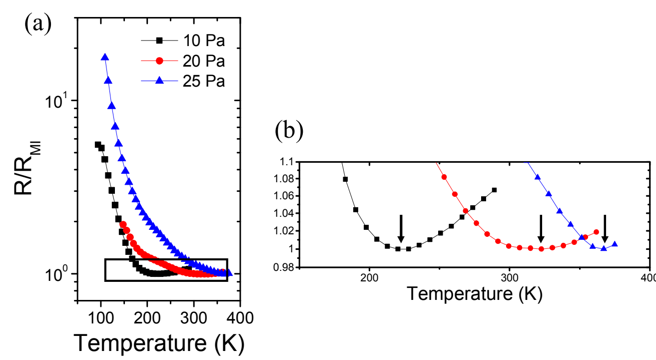

Figure 2 (a) SNNO films resistance as the function of temperature with different growth oxygen pressure. The resistance is normalized to its minimum value reached at T_{MI}. (b) The larger version of the area outlined in black in (a). The arrows indicate the T_{MI}.

Fig. 2 (a) shows the temperature dependent resistance of the SNNO/LAO films in the temperature range of 100 K – 400 K. The resistance is normalized to its minimum value reached at the T_{MI}. Fig. 2 (b) presents the zoom-in range around the transition points. It is obvious that all the SNNO films exhibit a clear MIT. The SNNO film deposited under 10 Pa has a fairly sharp MIT with T_{MI} at 220 K. The SNNO films deposited under 20 Pa and 25 Pa exhibit a smoother MIT with T_{MI} at 320 K and 356 K, respectively. It is clear that the decrease of deposition oxygen pressure strongly affects the MIT of the SNNO films, i.e., shifting the T_{MI} to lower temperature.

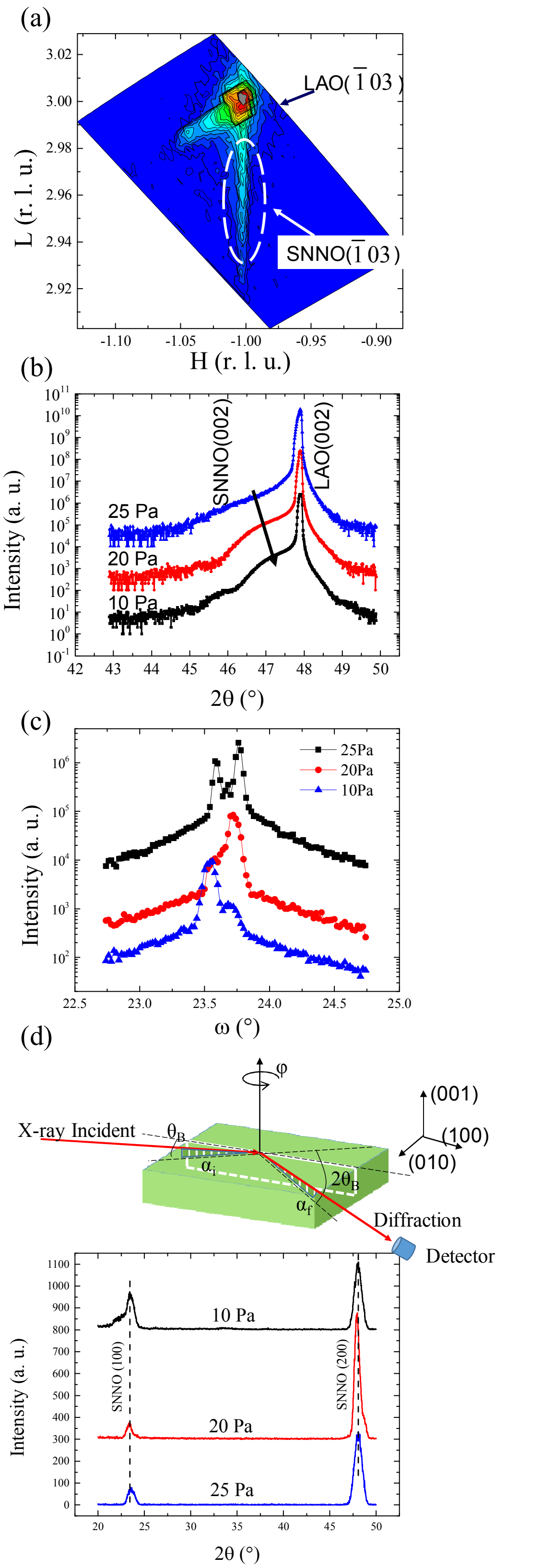

Figure 3 (a) Reciprocal space map around ($\bar{1}03$) reflection for the 20 Pa sample. (b) High-resolution X-ray θ-2θ scans around the (002) reflection and (b) the corresponding rocking curves across the SNNO (002) peak. (d) Schematic illustration of in-plane GIXRD geometry and GIXRD results for a series of SNNO films.

To verify whether the significant decrease of T_{MI} is due to the change of crystalline quality and lattice parameters of the films, high resolution synchrotron radiation XRD was carried out at NSRL. The full range x-ray θ-2θ scans indicate the pure phase and highly orientation of the SNNO films (not shown here). Fig. 3 (a) shows a typical non-specular ($\bar{1}03$) reciprocal space map (RSM) of the film deposited under 20Pa oxygen pressure. The RSM shows that the in-plane lattice parameter of the film is almost equal to the lattice parameter of LAO substrate (the difference is far less than the theoretical value of 0.4%), indicating that the films are fully compressive strained to the LAO substrate. Fig. 3 (b) shows the fine θ-2θ scans around the (002) diffraction peak. The diffraction peaks of SNNO shift slightly toward higher angles as decrease of the oxygen pressure, indicating a slight decrease of the out-of-plane lattice parameters. In Fig. 4, the out-of-plane lattice parameters derived from these θ-2θ scans are presented, where the difference between the parameters is less than 0.1%. Please note that all the out-of-plane lattice parameters are little larger than the theoretical one for bulk SNNO (pseudocubic, a_p is calculated to be 0.38 nm [13]), which is consistent with the in-plane compressive strain induced by the LAO substrate. Fig. 3 (c) plotted the rocking curves with 2θ centred on the SNNO films (002) peak. The FWHM for the 25-Pa, 20-Pa and 10-Pa films are 0.044°±0.001°, 0.077°±0.002° and 0.091°±0.002°, corresponding lateral crystalline size of 449 nm, 256 nm, and 217 nm, respectively. The presence of multi-peak in the rocking curve is due to the twinning nature of LAO substrate, which is a ubiquitous phenomenon for this substrate. To further investigate the evolution of the lattice parameters, GIXRD were performed to measure the in-plane lattice parameters. GIXRD geometry is illustrated in Figure 3 (d) and the angles were set to $\alpha_i = \alpha_f = 0.297°$, which corresponds to the critical angle of the film-air interface measured by XRR. GIXRD patterns along [*h*00] direction is shown in Fig. 3 (d), where only the (100) and (200) reflections of SNNO were observed. As numerically presented in Fig. 4, all the in-plane lattice parameters of these films are almost the same as that of the LAO substrate, which is consistent with the RSM result. The above structure analysis results indicate that the SNNO films deposited at varied oxygen pressure have almost the same strain status. Although there is still slight difference between the out-of-plane lattice parameters, such small lattice difference will not induce an obvious change in the metal-insulator transition, according to previous literatures [7, 11, 12]. Therefore, it indicates that the change of film lattice constant (strain state) is not the major origination of the shift of T_{MI}.

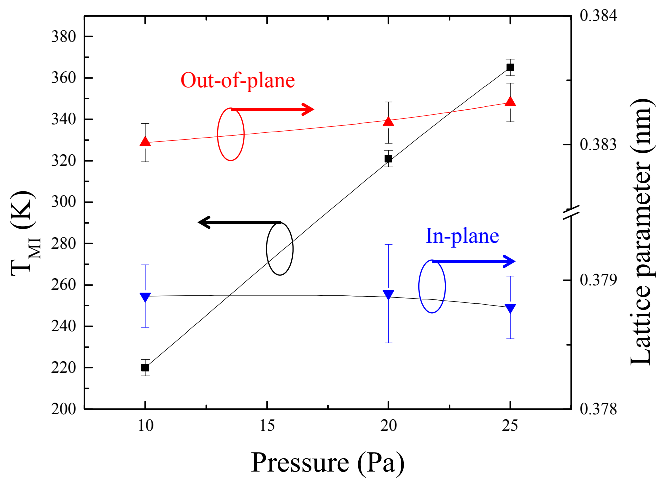

Figure 4 Film T_{MI} and lattice parameters as a function of the growth oxygen pressure.

Another hypothesis is that the pressure-induced oxygen vacancy is the cause of the change of T_{MI}. According to reports in the literatures, oxygen vacancies will often expand the out-of-plane lattice parameter in thin films [22-25], which is slightly different with our measurement. Fig. 5 schematically shows the oxygen vacancies effect on the lattice parameters in a compressively strained thin film. For a perovskite ABO_3 epitaxial thin film below critical thickness, the BO_6 octahedron can distort to relax the strain varied with increasing oxygen vacancies in a way of keeping the in-plane lattice parameter and stretching the out-of-plane lattice parameter [25-28]. However, the octahedral rotation should also be considered for oxygen-vacancy induced anisotropic crystal field in *Re*NiO_3. Oxygen vacancies appearing in the film will result in an anisotropic local coordination around Ni, which will boost the NiO_6 octahedral rotation commonly appearing in perovskite *Re*NiO_3. As a result, such octahedral rotation will change the Ni-O-Ni bond angle and slightly decrease the lattice constants. A little exaggerated schematic diagram of this effect is plotted in Fig. 5 (b). In our case, considering octahedral distortion and rotation, as well as the good lattice-match between the SNNO film and LAO substrate, the slightly increased lattice constant with the increase of growth oxygen pressure is reasonable.

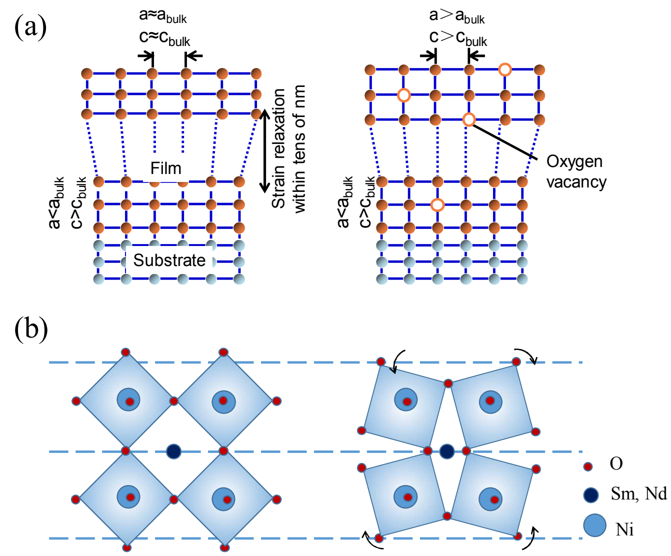

Figure 5 (a) Schematic diagram of oxygen vacancies effect on the lattice parameters in a compressive strained thin film. (b) Out-of-plane lattice parameter decrease with the Ni-O-Ni bond angle reduction.

In order to sustain the charge neutrality, oxygen vacancies in the film will be compensated by a change of the oxidation state of the nickel cation, from Ni^{3+} to Ni^{2+} [29]. The Ni $2p_{3/2}$ XPS spectra of films deposited at 10 Pa, 20 Pa and 25 Pa are shown in Fig. 6. The appearance of Ni^{2+} peak proves the existence of oxygen vacancy in the film. Although XPS result cannot be used to quantitatively determine the ion ration in the film, the measured Ni^{2+}/Ni^{3+} ratios for our 10Pa-, 20Pa-, 25Pa- samples are 0.29±0.01, 0.24±0.01, and 0.23±0.01, respectively, indicating the trend that more oxygen vacancy was induced at low growth oxygen pressure. In this study, oxygen vacancies decrease the T_{MI} of *Re*NiO_3, which is consistent with Ref 30 and 31. However, the detailed mechanism is still not clear as stated in Ref 1. In addition, it is generally accepted that charge disproportionation at the Ni site in the form of $Ni^{3+\delta}$-O^{2-}-$Ni^{3-\delta}$ contributes to the insulating state of *Re*NiO_3 [32-36], which encourage us to suggest that it's harder to form the $Ni^{3+\delta}$-O^{2-}-$Ni^{3-\delta}$ charge order when more oxygen vacancies appear in the *Re*NiO_3 films and therefore keeps the films in metallic state.

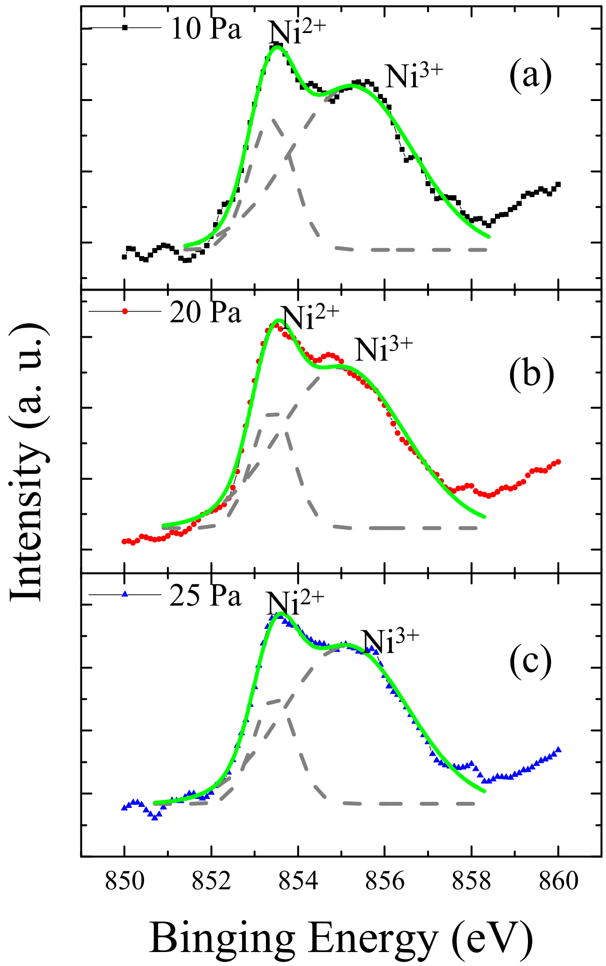

Figure 6 Ni $2p_{3/2}$ XPS spectra of (a) 10 Pa, (b) 20 Pa and (c) 25 Pa SNNO/LAO films. The peaks associated with Ni^{2+} and Ni^{3+} are indicated.

Conclusions

In summary, ultrathin coherently epitaxial $Sm_{0.6}Nd_{0.4}NiO_3$ films were fabricated on (001) $LaAlO_3$ by PLD under various growth oxygen pressure. It was found that the T_{MI} of the SNNO films remarkably decreases with the decrease of the growth oxygen pressure, while the strain state varied slightly. The XPS results indicate that oxygen vacancies induced by lower growth oxygen pressure seem to be the main cause of such phenomena. This work rules out the strain effect from the complicated factors affecting the MIT of *Re*NiO_3 film.

Acknowledgements

This work was supported by the National Basic Research Program of China (2010CB934501, 2012CB922004), the National Natural Science Foundation of China. The authors thank beam line BL14B of SSRF and U7B of NSRL for providing the beam time. HL Huang and YJ Yang acknowledge the Fundamental Research Funds for the Central Universities.

Notes and references

[a] Department of Physics, University of Science and Technology of China, Hefei, Anhui 230026, China
[b] National Synchrotron Radiation Laboratory & Collaborative Innovation Centre of Chemistry for Energy Materials, University of Science and Technology of China, Hefei, Anhui 230026, China
[c] CAS Key Laboratory of Materials for Energy Conversion, Department of Materials Science and Engineering, University of Science and Technology of China, Hefei, Anhui 230026, China
† Corresponding Authors: zlluo@ustc.edu.cn, cgao@ustc.edu.cn.

1. G. Catalan, *Phase Transitions*, 2008, **81**, 729.
2. D. Khomskii, *Physics*, 2009, **2**, 20.
3. S. W. Cheong and M. Mostovoy, *Nat. Mater.* 2007, **6**, 13.
4. J. van den Brink and D. I. Khomskii, *J. Phys. Condens. Matter,* 2008, **20**, 434217.
5. I. V. Nikulina, M. A. Novojilova, A. R. Kaulb, S. N. Mudretsovab, S. V. Kondrashov, *Materials Research Bulletin*, 2004, **39**, 775.
6. Z. Yang, C. Ko, and S. Ramanathan, *Annual Review of Materials Research*, 2011, **41**, 337.
7. R. Scherwitzl, P. Zubko, I. G. Lezama, S. Ono, A. F. Morpurgo, G. Catalan, and J. M. Triscone, *Adv. Mater.* 2010, **22**, 5517.
8. J. S. Zhou, J. B. Goodenough, B. Dabrowski, *Phys. Rev. Lett.* 2005, **94**, 226602.
9. J. Shi, S. D. Ha, Y. Zhou, F. Schoofs and S. Ramanathan, *Nat. Commun.* 2013, **4**, 2676.
10. H. L. Huang, Z. L. Luo, Y. J. Yang, Y. Yun, M. M. Yang, D. C. Meng, H. B. Wang, S. X. Hu, J. Bao, Y. L. Lu, C. Gao, *AIP Advances*, **4**, 057102 (2014).
11. J. Liu, M. Kargarian, M. Kareev, B. Gray, P. J. Ryan, A. Cruz, N. Tahir, Y. D. Chuang, J. H. Guo, J. M. Rondinelli, J. W. Freeland, G. A. Fiete and J. Chakhalian, *Nat. Commun.* 2013, **4**, 2714.
12. A. Tiwari, C. Jin, and J. Narayan, *Appl. Phys. Lett.* 2002, **80**, 4039.
13. A. Ambrosini and J. Hamet, *Appl. Phys. Lett.* 2003, **82**, 727.
14. R. Mahesh, K. R. Kannan, and C. N. Rao, *Journal of Solid State Chemistry*, 1995, **114**, 294.
15. A. Tiwari, K. P. Rajeev, Solid State Communications, 1999, **109**, 119.
16. G. H. Aydogdu, S. D. Ha, B. Viswanath, and S. Ramanathan, *J. Appl. Phys.* 2011, **109**, 124110.
17. Y. Kumar, R. J. Choudhar, S. K. Sharma, M. Knobel, and R. Kumar, *Appl. Phys. Lett.* 2012, **101**, 132101.
18. G. Catalan, R. M. Bowman, and J. M. Gregg, *Phys. Rev. B*, 2000, **62**, 7892.
19. G. I. Meijer, *Science*, 2008, **319**, 1625.
20. A. C. Zeppenfeld, S. L. Fiddler, W. K. Ham, B. J. Klopfenstein, C. J. Page, *J. Am. Chem. Soc.* 1994, **116**, 9158.
21. V. Holy, U. Pietsch, T. Baumbach, *High-Resolution X-Ray Scattering from Thin Films and Multilayers*, Springer: New York, 1999, Vol. 149.

22. T. Petrisor Jr., M. S. Gabor, A. Boulle, C. Bellouard, C. Tiusan, O. Pana and T. Petrisor, *J. Appl. Phys.* 2011, **109**, 123913.
23. P. Orgiani, C. Aruta, R. Ciancio, A. Galdi, and L. Maritato, *Appl. Phys. Lett*. 2009, **95**, 013510.
24. M. Kanai, H. Tanaka, T. Kawai, *Phys. Rev. B*, 2004, **70**, 125109.
25. P. Orgiani, A. Y. Petrov, R. Ciancio, A. Galdi, L. Maritato, and B. A. Davidson, *Appl. Phys. Lett.* 2012, **100**, 042404.
26. Lee, D., A. Yoon, S. Y. Jang, J.-G. Yoon, J.-S. Chung, M. Kim, J. F. Scott, and T. W. Noh, *Phys. Rev. Lett.* 2011, **107**, 057602.
27. Z. T. Xu, K. j. Jin, L. Gu, Y. L. Jin, C. Ge, C. Wang, H. Z. Guo, H. B. Lu, R. Q. Zhao, and G. Z. Yang, *Small*, 2012, **8**, 1279.
28. J. M. Rondinelli, and N. A. Spaldin, *Adv. Mater.* 2011, **23**, 3363.
29. S. D. Ha, G. H. Aydogdu, S. Ramanathan, *Appl. Phys. Lett.* 2011, **98**, 012105.
30. S. D. Ha, M. Otaki, R. Jaramillo, A. Podpirka, S. Ramanathan, *J. Solid State Chem.* 2012, **190**, 233.
31. X. K. Lian, F. Chen, X. L. Tan, L. F. Wang, X. F. Xuan, G. Y. Gao,S. W. Jin, and W. B. Wu, *AIP Advances*, **3**, 062133 (2013).
32. U. Staub, G. I. Meijer, F. Fauth, R. Allenspach, J. G. Bednorz, J. Karpinski, S. M. Kazakov, L. Paolasini, and F. d'Acapito, *Phys. Rev. Lett.* 2002, **88**, 126402.
33. J. A. Alonso, M. J. Martínez-Lope, I. A. Presniakov, A. V. Sobolev, V. S. Rusakov, A. M. Gapochka, G. Demazeau, M. T. Fernández-Díaz, *Phys. Rev. B* 2013, **87**, 184111.
34. J. A. Alonso, M. J. Martínez-Lope, M. T. Casais, J. L. García-Muñoz, M. T. Fernández-Díaz, *Phys. Rev. B* 2000, **61**, 1756.
35. J. A. Alonso, J. L. García-Muñoz, M. T. Fernández-Díaz, M. A. G. Aranda, M. J. Martínez-Lope, and M. T. Casais, *Phys. Rev. Lett.* 1999, **82**, 3871.
36. M. Zaghrioui, A. Bulou, P. Lacorre, and P. Laffez, *Phys. Rev. B* 2001, **64**, 081102.